Anisotropic Mean Flow Enhancement and Anomalous Transport of Finite-Size Spherical Particles in Turbulent Flows

Alessandro Chiarini, Ianto Cannon, and Marco Edoardo Rosti*
Complex Fluids and Flows Unit, Okinawa Institute of Science and Technology Graduate University, 1919-1 Tancha, Onna-son, Okinawa 904-0495, Japan

(Received 1 August 2023; accepted 19 December 2023; published 2 February 2024)

We investigate the influence of dispersed solid spherical particles on the largest scales of the turbulent Arnold-Beltrami-Childress (ABC) flow. The ABC flow is an ideal instance of a complex flow: it does not have solid boundaries, but possesses an inhomogeneous and three-dimensional mean shear. By tuning the parameters of the suspension, we show that particles modulate the largest scales of the flow toward an anisotropic, quasi-two-dimensional and more energetic state. In this regime, particles move along quasistraight trajectories and exhibit anomalous transport.

DOI: 10.1103/PhysRevLett.132.054005

Particle-laden turbulent flows have attracted the attention of many scholars over the last decades. Their significance goes beyond a fundamental interest and encompasses several applications such as blood flow in the human body, the food industry, and pyroclastic flows [1–3]. Also, the modulation of the mean flow and the enhancement or attenuation of turbulence due to particles are relevant in both environmental [4] and industrial flows [5]. However, although this is a classical problem in fluid mechanics since the seminal work by Tsuji andMorikawa [6], the multiscale mechanism governing the fluid-particle interaction is still an open question. In particular, the ability of suspensions of solid particles to modify and control the largest scales of a generic and complex flow is unclear.

The presence of the solid phase alters the momentum of the flow, and may result in modulation of the carrier fluid [7,8]. When the suspension is dilute enough, the fluid phase can be considered unaltered by the presence of the particles. Instead, when the suspension is nondilute, the fluid phase undergoes macroscopic changes in a way that depends on several parameters, such as, for example, the size and density of the particles, and the volume and mass fractions of the suspension [9,10]. Over the last years, the solid-fluid interaction in particle-laden turbulent flows has been the subject of several studies in various flows, ranging from homogeneous and isotropic flows [11] to wall-bounded flows [12]. Nevertheless, the influence of the solid phase on the largest scales of a generic and complex flow has not yet been satisfactorily addressed, and the accurate characterization of the underlying physics still requires significant effort. Here, we aim to address the following questions. How do suspensions of solid particles modulate the largest and most energetic scales of the flow in the presence of an inhomogeneous mean shear? Is it possible to use particles to effectively modify and control the mean flow?

In order to answer these questions, in this Letter we study the modulation of the turbulent Arnold-Beltrami-Childress (ABC) flow by finite-size particles, with a focus on the largest scales. In a Cartesian reference system the laminar ABC flow is L periodic in the three x, y, and z directions, with a velocity field $\boldsymbol{u} = (u, v, w)$ that depends on four real parameters V_o, A, B, and C, i.e.,

$$\begin{aligned} u/V_o &= A\sin\left(\frac{2\pi}{L}z\right) + C\cos\left(\frac{2\pi}{L}y\right), \\ v/V_o &= B\sin\left(\frac{2\pi}{L}x\right) + A\cos\left(\frac{2\pi}{L}z\right), \\ w/V_o &= C\sin\left(\frac{2\pi}{L}y\right) + B\cos\left(\frac{2\pi}{L}x\right); \end{aligned} \tag{1}$$

A, B, and C are bounded between 0 and 1 and determine the shape of the flow, while V_o determines the magnitude. Here, we consider the turbulent ABC flow, which is obtained by forcing the incompressible Navier-Stokes equations with the ABC forcing with $A = B = C = 1$ [13] (see Fig. 1). This provides an ideal instance of a complex turbulent flow with a three-dimensional (3D) mean field and an inhomogeneous mean shear, such as flow past an object or in a curved pipe. Because of the lack of solid boundaries, in the ABC flow the complex flow structures induced by the presence of a wall are avoided. Thus, the particle-laden turbulent ABC flow allows us to isolate the

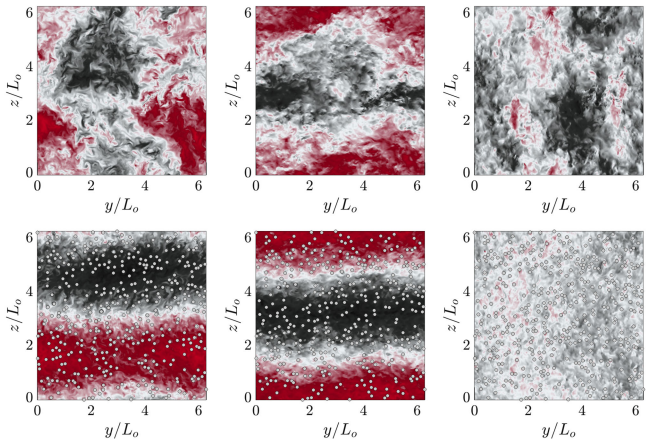

FIG. 1. Instantaneous velocity field in the $x = L/2$ plane for the (top) single-phase case and the (bottom) particulate case with $D/L \approx 0.02$ and $M = 0.6$. Left: u; center: v; right: w. The symmetric black-to-red color map goes from $-9 \leq u_i/U_o \leq 9$ [14]; see Supplemental Material [15]. We denote with z the direction orthogonal to the trajectories' plane [21]; see Supplemental Material [15].

influence of the particles on the large-scale motions, that in wall-bounded flows might be hidden by the complex near-wall phenomenology. In this idealized framework, we show that nondilute suspensions of solid particles can substantially modify the structure of the mean flow. When tuning their size and density, indeed, particles modulate the largest scales of the flow toward an anisotropic, almost two-dimensional (2D) and more energetic state (see Fig. 1). Intriguingly, we show that this happens in the presence of a sustained 3D external forcing, whose effect is overcome by the presence of the solid phase. This paves the way for the use of solid particles to control complex 3D flows.

To tackle this problem, we have performed 3D direct numerical simulations of the flow within a triperiodic box of size L, with dispersed particles of various finite sizes, that lie within the inertial range of turbulence. The fluid and the solid dynamics are fully resolved, and coupled with an immersed boundary method [22]. The external ABC forcing is set to achieve, in the single-phase case, a microscale Reynolds number of $\mathrm{Re}_\lambda = u'\lambda/\nu \approx 435$, where u' is the root mean square of the velocity fluctuations and λ is the Taylor length scale [15]. The particle diameter is varied between $0.0104 \leq D/L \leq 0.0796$. For each particle size, the number of particles is set to provide a volume fraction of $\Phi_V \approx 0.08$, which is large enough for the suspension to be nondilute and small enough for the particle-particle interactions to be subdominant. Finally, the ratio between the density of the particles and the fluid is varied between $1.3 \leq \rho_p/\rho_f \leq 105$, to consider both light and heavy particles, yielding a variation of the mass fraction between $0.1 \leq M \leq 0.9$. See Supplemental Material for the definitions of the dimensionless groups.

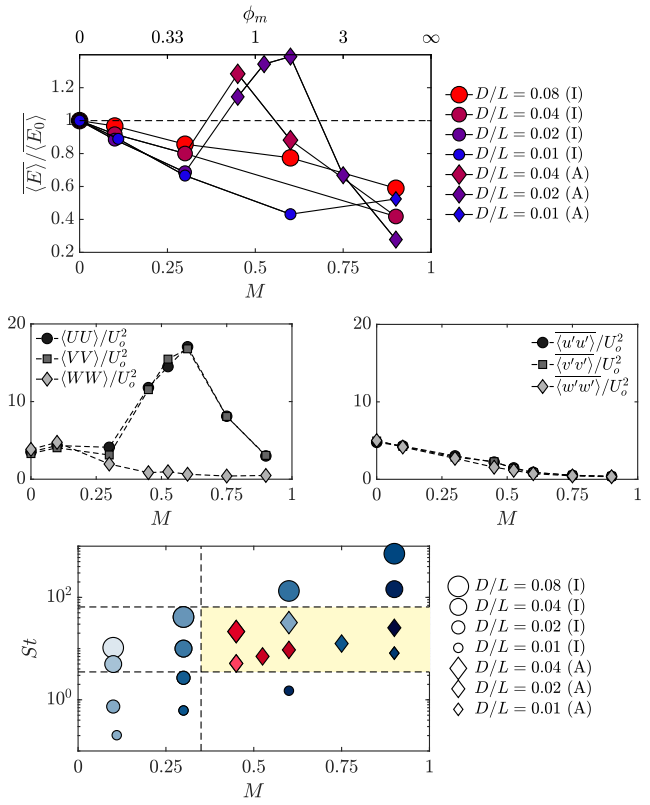

FIG. 2. Modulation of the flow energy by finite-size solid particles. Top panel: total kinetic energy of the flow as a function of the mass fraction M and of the mass loading ϕ_m, for different particle size. E_0 is the total kinetic energy of the single-phase flow. Circles and diamonds refer to the isotropic (I) and anisotropic (A) regimes. In the central panels the influence of the solid phase on the mean and fluctuating field is isolated for $D/L \approx 0.02$. Center left: variance of the mean velocity components. Center right: variance of the fluctuating velocity components. Bottom panel: modulation of the kinetic energy of the flow as a function of M and Stokes number St. Blue symbols are for $\overline{\langle E \rangle} < \overline{\langle E_0 \rangle}$, red symbols for $\overline{\langle E \rangle} > \overline{\langle E_0 \rangle}$ with the divergent blue-to-red color map being for $0.25 \leq \overline{\langle E \rangle}/\overline{\langle E_0 \rangle} \leq 1.75$. The shaded region shows the anisotropic regime.

Figure 2 shows that the modulation of the carrier ABC flow changes with the size and density of the particles. In the top panel, we plot the total kinetic energy of the flow $\overline{\langle E(\boldsymbol{x},t) \rangle}$ for different values of D and M, where $E(\boldsymbol{x},t) = |\boldsymbol{u}(\boldsymbol{x},t)|^2/2$, while $\langle \cdot \rangle$ and $\overline{\cdot}$ indicate average along homogeneous directions and in time, respectively. Overall, the total energy decreases while reducing D and increasing M, in agreement with the findings of previous authors [11,23–25]. However, the trend is nonmonotonic, and the large increase of $\overline{\langle E \rangle}$ for $M \gtrsim 0.45$ and $D/L \lesssim 0.04$ shows that the solid phase modulates the carrier flow in a way that sharply changes with the density of the particles. Interestingly, solid suspensions of particles with $0.02 \lesssim D/L \lesssim 0.04$ and $0.45 \leq M \leq 0.6$ enhance the total energy of the carrier flow with respect to the single-phase case. In

the central panels of Fig. 2, we use a temporal average to isolate the influence of the solid phase on the large and small scales of the carrier flow. We consider the $D/L \approx 0.02$ particulate cases and, after decomposing the velocity field into its temporal mean $\boldsymbol{U}(\boldsymbol{x}) = \overline{\boldsymbol{u}(\boldsymbol{x},t)}$ and fluctuations $\boldsymbol{u}'(\boldsymbol{x},t) = \boldsymbol{u}(\boldsymbol{x},t) - \boldsymbol{U}(\boldsymbol{x})$, we plot the variances of their three components [14]. Light particles ($M \leq 0.3$) modulate the flow without introducing a preferential direction, and attenuate the energy of the fluid phase by modifying the mean and fluctuating fields in an isotropic way. Indeed, here $\langle UU \rangle \approx \langle VV \rangle \approx \langle WW \rangle$ and $\overline{\langle u'u' \rangle} \approx \overline{\langle v'v' \rangle} \approx \overline{\langle w'w' \rangle}$. Heavier particles ($M \geq 0.45$), instead, modulate differently the mean and fluctuating fields. They continue to attenuate the energy of the fluctuations in an isotropic way, but modulate the mean field toward an anisotropic, quasi-2D and more energetic state. In this case, $\langle UU \rangle \approx \langle VV \rangle \gg \langle WW \rangle$ [21], while $\overline{\langle u'u' \rangle} \approx \overline{\langle v'v' \rangle} \approx \overline{\langle w'w' \rangle}$. The increase of the total flow energy observed for $0.45 \leq M \leq 0.6$ is thus entirely due to the mean-flow energy enhancement.

The anisotropic state is observed in a limited portion of the space of mass fraction M and Stokes number St, i.e., $5 \lesssim \mathrm{St} \lesssim 60$ and $M \gtrsim 0.4$ (see the bottom panel of Fig. 2). The anisotropy of the large scales is indeed favored by the motion of the particles when, due to their inertia, they tend to move along straight trajectories. Particles with $\mathrm{St} \lesssim 5$ follow the complex fluid motion and hence do not significantly modify the flow. However, for $5 \lesssim \mathrm{St} \lesssim 60$, inertia causes the particle trajectories to straighten, causing the fluid motion to reorganize into a quasi-2D state. When St further increases, the particles become less responsive to the fluid motion, and the 2D state does not develop. Note that the isotropic flow modulation observed for $\mathrm{St} \gtrsim 60$ is consistent with the limit of infinite inertia: when $\mathrm{St} \to \infty$, the particles do not move, and the quasi-2D flow does not arise. The dependence of the flow modulation on M shows that the emergence of the anisotropic state requires a strong enough backreaction of the particles to the fluid phase. Also, the ability of the particles to modulate the largest scales of the carrier flow strongly depends on the ratio D/L. In fact, the strongest flow modulation (and largest mean-flow enhancement) is observed for the intermediate $D/L \approx 0.02$, while the effect is lower for both smaller and larger particles. For $D \ll L$, indeed, particles have a small inertia, follow the fluid, and do not favor the flow two-dimensionalization. For $D \approx L$, instead, the motion of the particles is only marginally influenced by the mean shear, as it is mainly driven by fluid velocity fluctuations with a length scale larger than their characteristic size. See Supplemental Material [15] for further discussions, and for the dependence of the anisotropic flow modulation on the inhomogeneous mean shear.

Next, we use Poincaré sections [26] to characterize the modulation of the mean flow $\boldsymbol{U}$. These are a 2D coding of a 3D dynamical system, in which one represents only the successive intersections of the mean-flow streamlines with

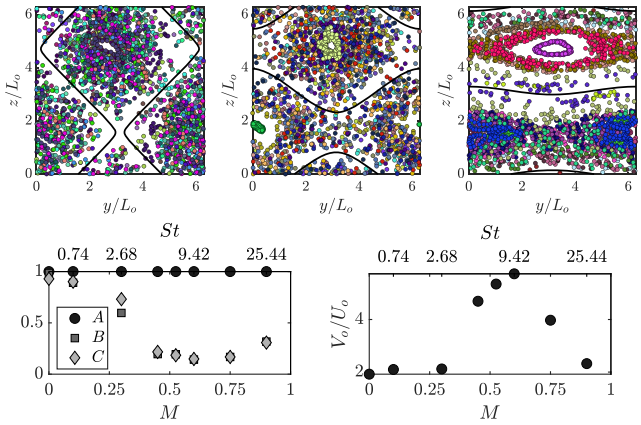

FIG. 3. Mean flow field for $D/L \approx 0.02$. Top: Poincaré section for the mean flow of the single-phase case (right) and of the particulate cases with $M = 0.3$ (center) and $M = 0.6$ (right). Twenty streamlines are considered, each identified by a different color. Bottom: variation with M and St of A, B, C, and V_o used in Eq. (1) to approximate the mean flow. Without losing generality we set that the maximum between A, B, and C is equal to 1 [15]. The black lines in the Poincaré sections are for $U = A\sin(z) + C\cos(y) = 0$ with A and C as in the bottom left panel.

one plane of the triperiodic domain. Figure 3 shows the $x = L/2$ Poincaré section for the mean flow of the turbulent single-phase case, and of the $D/L \approx 0.02$ particulate cases with $M = 0.3$ and $M = 0.6$. For each streamline many successive intersections with the $x = L/2$ plane are represented. At first glance, the Poincaré maps show that points associated with the same streamline are found to span a narrower range of z as the flow anisotropy increases. This confirms that in the anisotropic regime, particles attenuate the W velocity component and modulate the mean field toward a quasi 2D state (see Fig. 2). The density of the points in the Poincaré section is proportional to the magnitude of the mean velocity component aligned with the direction perpendicular to the plane [27]. In the laminar case, indeed, the density of the points in the $x = L/2$ Poincaré plane falls to zero along the $U/V_o = \sin(z/L_o) + \cos(y/L_o) = 0$ line (see Fig. 5 of Supplemental Material [15]). A similar pattern is observed for the turbulent single-phase case. In fact, a remarkable property of the ABC flow is that even in the turbulent regime, the mean velocity has nearly the laminar ABC profile, as observed by others for the Kolmogorov flow [28,29]. In the particulate cases, the scenario progressively changes with M. Interestingly, the solid phase modulates the mean flow in a way that it resembles a generic ABC flow, but with different values of A, B, C, and V_o. In view of this, the bottom panels of Fig. 3 report the coefficients of the generic ABC flow that best approximates the mean flow for $D/L \approx 0.02$ and $0.1 \leq M \leq 0.9$ [15]. As M (and St) increases, $A = 1$ remains constant, while $B \approx C$ decrease and reach a minimum for $M = 0.6$ ($\mathrm{St} \approx 9.42$) where the flow anisotropy is maximum. In this case, $A \gg B \approx C$ and the streamlines

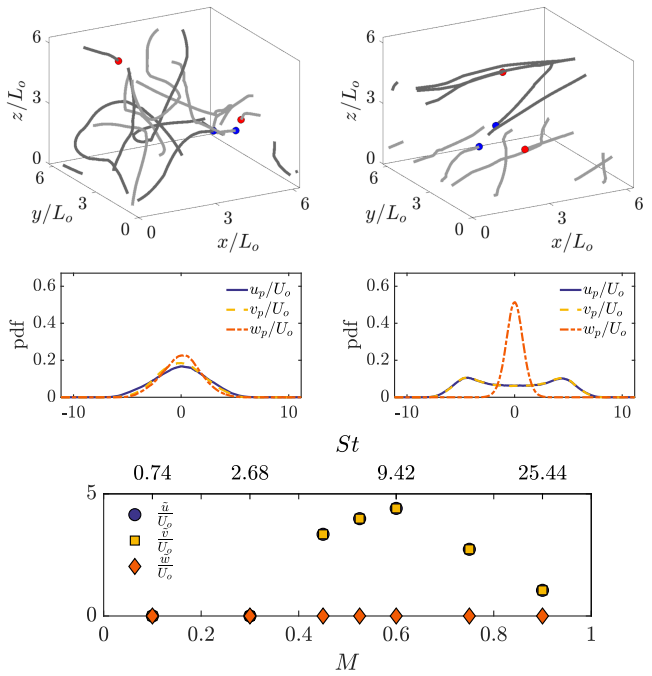

FIG. 4. Particle dynamics for $D/L \approx 0.02$. Top panels: two representative trajectories for (left) $M = 0.3$ and (right) $M = 0.6$; the red (blue) circle indicate the beginning (end) of the trajectories. Central panels: probability density functions for (left) $M = 0.3$ and (right) $M = 0.6$. Bottom panel: dependence of the modes $\tilde{u}_i$ of the probability density functions on M and St.

of the mean flow are almost straight lines that lay in the x-y planes, as $(U, V, W) \sim [\sin(z/L_o), \cos(z/L_o), 0]$. Thus, particles with $0.45 \leq M \leq 0.9$ and $5.13 \lesssim \mathrm{St} \lesssim 25.45$ attenuate the W velocity component, and the mean flow approaches an anisotropic and 2D state, almost losing its dependence on x and y; see the black lines in Fig. 3. V_o sharply increases for $M \geq 0.45$ ($\mathrm{St} \gtrsim 5.13$), in agreement with the enhancement of the mean-flow energy shown in Fig. 2. This anisotropic and almost 2D state resembles the bifurcated $\mathcal{A}_2$ state of the single-phase laminar ABC flow found by Podvigina and Pouquet [13], spontaneously emerging at lower Reynolds numbers. Thus, it appears that the presence of particles with $5 \lesssim \mathrm{St} \lesssim 60$ and $M > 0.3$, and their tendency to follow straight trajectories, changes the stability of the system, enabling thus the occurrence of an anisotropic $\mathcal{A}_2$-like state at the large scales also for these larger Re [15].

To further investigate the fluid-solid interaction, Figs. 4 and 5 characterize the particles' dynamics for $D/L \approx 0.02$. In the isotropic regime ($M \leq 0.3$ and $\mathrm{St} \lesssim 2.68$), particles are able to follow the intricate ABC cellular forcing, and exhibit complex trajectories as expected by the chaotic Lagrangian structure of the ABC flow [27]. In this case, the particles do not select a preferential direction, and explore the entire computational domain. Indeed, the probability density functions of the three velocity components almost collapse, exhibiting a symmetric unimodal distribution.

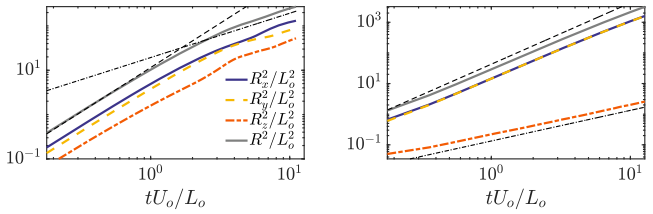

FIG. 5. Particle mean squared displacement $R^2(t)$ for $D/L \approx 0.02$. Left: $M = 0.3$. Right: $M = 0.6$. The thin dashed line represents t^2, while the thin dash-dotted line t.

On the contrary, in the anisotropic regime ($0.45 \leq M \leq 0.9$ and $5.13 \lesssim \mathrm{St} \lesssim 25.44$), the particles move along almost straight trajectories with $u_p \approx v_p \gg w_p$. The direction of the trajectories of the particles in the x-y plane changes with z, in agreement with the fact that $A \gg B \approx C$, and $U \sim \sin(z/L_o)$ and $V \sim \cos(z/L_o)$. As a result, the in-plane components of the particle velocity exhibit a symmetric bimodal distribution, and the modes $\pm\tilde{u}_p$ and $\pm\tilde{v}_p$ change with the density of the particles (see bottom panel of Fig. 4).

Figure 5 shows the mean squared displacement of the particles, $R(t)^2 = \langle |\boldsymbol{x}_p(t) - \boldsymbol{x}_p(0)|^2 \rangle_p$; here, $\langle \cdot \rangle_p$ indicates average over particles. The particle motion is diffusive (ballistic) when $R^2(t) \sim t^\alpha$ with $\alpha = 1$ (2). As expected, in the isotropic regime, particles show ballistic motion for short times, while at large times, their motion becomes uncorrelated under the action of the random velocity fluctuations, and they exhibit a diffusive process; see the $M = 0.3$ case in the left panel. In the anisotropic regime, instead, particles exhibit anomalous transport with $1 < \alpha < 2$ at large times; see the $M = 0.6$ case in the right panel. The scaling of the anomalous transport slightly changes with the density of the particles in the $1.6 \lessapprox \alpha \lessapprox 1.75$ range, increasing as the particles' motion becomes more coherent and their trajectories more straight. Note that considering the z direction alone, i.e., $R_z(t)^2 = \langle |z_p(t) - z_p(0)|^2 \rangle_p$, the diffusive transport with $\alpha \approx 1$ is recovered also for heavy particles.

To conclude, we have shown that in the presence of a 3D and inhomogeneous mean shear, solid particles can substantially modify the structure of the largest scales of the flow. By tuning the size and the density of the particles, nondilute suspensions can modulate the largest scales of the flow toward an anisotropic, almost 2D and more energetic state, while preserving isotropy at smaller scales. The ability of solid particles to modify the large-scale flow may pave the way for their use in flow-control purposes. For example, the cooling and cleaning effects of oil in an engine are undermined by recirculating regions in the flow [30,31]. We showed that adding particles can potentially eliminate such recirculating regions, improving engine efficiency and lifetime. Also, our results show that there is a specific regime in which the ballistic motion of the particles is favored over diffusive motion, with relevance for drug delivery and pollen dispersal [32,33].

The research was supported by the Okinawa Institute of Science and Technology Graduate University (OIST) with subsidy funding from the Cabinet Office, Government of Japan. The authors acknowledge the computer time provided by the Scientific Computing section of Research Support Division at OIST.

*marco.rosti@oist.jp

[1] F. De Lillo, M. Cencini, W. M. Durham, M. Barry, R. Stocker, E. Climent, and G. Boffetta, Turbulent fluid acceleration generates clusters of gyrotactic microorganisms, Phys. Rev. Lett. **112**, 044502 (2014).

[2] E. C. P. Breard, G. Lube, J. R. Jones, J. Dufek, S. J. Cronin, G. A. Valentine, and A. Moebis, Coupling of turbulent and non-turbulent flow regimes within pyroclastic density currents, Nat. Geosci. **9**, 767 (2016).

[3] F. Falkinhoff, M. Obligado, M. Bourgoin, and P. D. Mininni, Preferential concentration of free-falling heavy particles in turbulence, Phys. Rev. Lett. **125**, 064504 (2020).

[4] A. Sengupta, F. Carrara, and R. Stocker, Phytoplankton can actively diversify their migration strategy in response to turbulent cues, Nature (London) **543**, 555 (2017).

[5] S. A. Ferreyra, S. Uehara, M. d. S. Ferreira, and O. Mian, *Engine Lubrication System for Oil Flow Reduction*, SAE Technical Paper 2011-36-0205 (SAE International, Warrendale, PA, 2011).

[6] Y. Tsuji and Y. Morikawa, LDV measurements of an air–Solid two-phase flow in a horizontal pipe, J. Fluid Mech. **120**, 385 (1982).

[7] S. Balachandar and J. K. Eaton, Turbulent dispersed multiphase flow, Annu. Rev. Fluid Mech. **42**, 111 (2010).

[8] L. Brandt and F. Coletti, Particle-laden turbulence: Progress and perspectives, Annu. Rev. Fluid Mech. **54**, 159 (2022).

[9] R. A. Gore and C. T. Crowe, Effect of particle size on modulating turbulent intensity, Int. J. Multiphase Flow **15**, 279 (1989).

[10] S. Elgobashi, An updated classification map of particle-laden turbulent flows, in *IUTAM Symposium on Computational Approaches to Multiphase Flow*, Fluid Mechanics and Its Applications, edited by S. Balachandar and A. Prosperetti (Springer Netherlands, Dordrecht, 2006), pp. 3–10.

[11] S. Oka and S. Goto, Attenuation of turbulence in a periodic cube by finite-size spherical solid particles, J. Fluid Mech. **949**, A45 (2022).

[12] P. Costa, F. Picano, L. Brandt, and W.-P. Breugem, Universal scaling laws for dense particle suspensions in turbulent wall-bounded flows, Phys. Rev. Lett. **117**, 134501 (2016).

[13] O. Podvigina and A. Pouquet, On the non-linear stability of the 1 : 1 : 1 ABC flow, Physica (Amsterdam) **75D**, 471 (1994).

[14] All quantities are made dimensionless with L_o and U_o, where $L_o = L/2\pi$ and $U_o = \sqrt{F_o L_o}$ with F_o denoting the intensity of the ABC forcing.

[15] See Supplemental Material at http://link.aps.org/supplemental/10.1103/PhysRevLett.132.054005 for more information, which includes Refs. [16–20].

[16] V. Eswaran and S. B. Pope, An examination of forcing in direct numerical simulations of turbulence, Comput. Fluids **16**, 257 (1988).

[17] Y. Tsuji, T. Kawaguchi, and T. Tanaka, Discrete particle simulation of two-dimensional fluidized bed, Powder Technol. **77**, 79 (1993).

[18] S. Pope, *Turbulent Flows* (Cambridge University Press, Cambridge, England, 2000).

[19] T. Kajishima, S. Takiguchi, H. Hamasaki, and Y. Miyake, Turbulence structure of Particle-laden flow in a vertical plane channel due to vortex shedding, JSME Int. J. B-Fluid T. **44**, 526 (2001).

[20] A. Monti, V. Rathee, A. Q. Shen, and M. E. Rosti, A fast and efficient tool to study the rheology of dense suspensions, Phys. Fluids **33**, 103314 (2021).

[21] Note that we denote with z the direction aligned with the mean-flow component that is attenuated by the particle modulation, corresponding to the direction orthogonal to the particle trajectories' plane.

[22] N. Hori, M. E. Rosti, and S. Takagi, An Eulerian-based immersed boundary method for particle suspensions with implicit lubrication model, Comput. Fluids **236**, 105278 (2022).

[23] A. Ten Cate, J. J. Derksen, L. M. Portela, and H. E. a. van Den Akker, Fully resolved simulations of colliding monodisperse spheres in forced isotropic turbulence, J. Fluid Mech. **519**, 233 (2004).

[24] M. Uhlmann and A. Chouippe, Clustering and preferential concentration of finite-size particles in forced homogeneous-isotropic turbulence, J. Fluid Mech. **812**, 991 (2017).

[25] S. Olivieri, I. Cannon, and M. E. Rosti, The effect of particle anisotropy on the modulation of turbulent flows, J. Fluid Mech. **950**, R2 (2022).

[26] H. Poincaré, *Les méthodes nouvelles de la mécanique céleste* (Gauthier-Villars, Paris, 1892).

[27] T. Dombre, U. Frisch, J. M. Greene, M. Hénon, A. Mehr, and A. M. Soward, Chaotic streamlines in the ABC flows, J. Fluid Mech. **167**, 353 (1986).

[28] V. Borue and S. A. Orszag, Numerical study of three-dimensional Kolmogorov flow at high Reynolds numbers, J. Fluid Mech. **306**, 293 (1996).

[29] S. Musacchio and G. Boffetta, Turbulent channel without boundaries: The periodic Kolmogorov flow, Phys. Rev. E **89**, 023004 (2014).

[30] R. Gamble, M. Priest, and C. Taylor, Detailed analysis of oil transport in the piston assembly of a gasoline engine, Tribol. Lett. **14**, 147 (2003).

[31] F. Concli and M. N. Mastrone, Advanced lubrication simulations of an entire test rig: Optimization of the nozzle orientation to maximize the lubrication capability, Lubricants **11**, 300 (2023).

[32] L. Hamaoui-Laguel, R. Vautard, L. Liu, F. Solmon, N. Viovy, D. Khvorostyanov, F. Essl, I. Chuine, A. Colette, M. A. Semenov, A. Schaffhauser, J. Storkey, M. Thibaudon, and M. M. Epstein, Effects of climate change and seed dispersal on airborne ragweed pollen loads in europe, Nat. Clim. Change **5**, 766 (2015).

[33] S. Ito, H. Rajabi, and S. N. Gorb, A ballistic pollen dispersal strategy based on stylar oscillation of *Hypochaeris radicata* (Asteraceae), J. Exp. Biol. **226**, jeb244258 (2023).